Journal of Power Sources 198 (2012) 229–235

Contents lists available at SciVerse ScienceDirect

Journal of Power Sources

journal homepage: www.elsevier.com/locate/jpowsour

Porous Li_2FeSiO_4/C nanocomposite as the cathode material of lithium-ion batteries

Zongmin Zheng, Yan Wang, Ai Zhang, Tianran Zhang, Fangyi Cheng, Zhanliang Tao*, Jun Chen*

Institute of New Energy Material Chemistry and Key Laboratory of Advanced Energy Materials Chemistry (Ministry of Education), College of Chemistry, Nankai University, Tianjin 300071, China

ARTICLE INFO

Article history:
Received 22 July 2011
Received in revised form 4 September 2011
Accepted 21 September 2011
Available online 29 September 2011

Keywords:
Polyanioic compounds
Carbon-coated nanocomposite
Porous structure
Cathode
Li-ion batteries

ABSTRACT

In this paper, we report on the facile preparation of porous Li_2FeSiO_4/C nanocomposites by tartaric acid-assisted sol–gel method and their electrochemical properties as the cathode materials of Li-ion batteries. The structure, morphology, and texture of the as-prepared samples are characterized by means of XRD, Raman, SEM, TEM/HRTEM, and N_2 adsorption/desorption techniques. The results show that the porous Li_2FeSiO_4/C nanocomposites are consisted of nanoparticles, which have been coated with in situ carbon on the surface. The electrochemical properties of the as-prepared Li_2FeSiO_4/C nanocomposites have been investigated using galvanostatic charge/discharge and cyclic voltammograms. It is found that porous Li_2FeSiO_4/C nanocomposite with 8.06 wt% carbon shows a high capacity of 176.8 mAh g^{-1} at 0.5 C in the first cycle and a reversible capacity of 132.1 mAh g^{-1} at 1 C (1 C = 160 mA g^{-1}) in the 50th cycle. This high capacity indicates that more than one electron reaction may be occurred. These results illustrate that the porous Li_2FeSiO_4/C nanocomposite with 8.06 wt% carbon is potential in the application of high-rate cathode material of Li-ion batteries.

1. Introduction

In the research area of lithium-ion batteries (LIBs), great efforts have been devoted to increasing the capacity and improving the security of the cathode materials [1]. Recently, the polyanionic compounds have attracted great interests for their stable structures and high capacities [2,3]. As a class of polyanionic compounds, Li_2FeSiO_4 holds a great promise as a potential cathode material because of its high specific theoretical capacity (166 mAh g^{-1} for one Li^+ exchange and 332 mAh g^{-1} if the second Li^+ exchange could be achieved) [4–8]. Furthermore, Li_2FeSiO_4 materials are also featured with virtues of low cost, high safety and nontoxicity. However, there are inherent disadvantages of Li_2FeSiO_4 such as low electronic conductivity and ion transmittability, which prevent the attainment of high electrochemical capacity and stable cyclability [9]. Recent studies show that both exploring porous nanostructured electrode and coating a conductive component have proven to be efficient strategies in enhancing the electrochemical performances of electrode materials [1,10]. Various methods such as ball milling [4,11] and citric acid-assisted sol–gel [9,12–14] have been successfully used to synthesize Li_2FeSiO_4/C nanoparticles. Among these ways, sol–gel method is a simple and effective way to prepare carbon coated nano-Li_2FeSiO_4, which can deliver a high capacity of 153.6 mAh g^{-1} at C/16 [13]. To further elevate the capacity and rate properties, researchers have attempted to observe porous and/or smaller-sized Li_2FeSiO_4/C through composite methods. For example, Li_2FeSiO_4/C composite with porous structure, which was prepared by sol–gel-assisted ball milling technique, delivered a discharge capacity of 155 mAh g^{-1} at 0.2 C [15]. Li_2FeSiO_4/C composite with the crystallite size of 40–80 nm, which was prepared by a hydrothermal-assisted sol–gel method, displayed a specific capacity of 125 mAh g^{-1} at 2 C [16]. It is thus that the preparation of Li_2FeSiO_4/C with further reduced particle size and porous structure should be interesting.

In this paper, we report on the synthesis of porous Li_2FeSiO_4/C nanocomposites and their promising electrochemical properties as the cathode materials of Li-ion batteries. A facile tartaric acid (TA) assisted sol–gel method was employed to prepare the porous Li_2FeSiO_4/C nanocomposites with the size around 30 nm. Through simply altering the molar ratio of TA/Li_2FeSiO_4, we obtained Li_2FeSiO_4/C composite with various contents of carbon coating. Furthermore, the as-synthesized porous Li_2FeSiO_4/C nanocomposites exhibited enhanced electronic conductivity and Li^+ diffusion coefficient as well as superior rate and cycling capabilities. The present results indicate that porous Li_2FeSiO_4/C nanocomposite with 8 wt% carbon coating on the surface is promising as the cathode material of Li-ion batteries.

* Corresponding authors. Tel.: +86 22 23506808; fax: +86 22 23506808.
E-mail addresses: taozhl@nankai.edu.cn (Z. Tao), chenabc@nankai.edu.cn (J. Chen).

0378-7753/$ – see front matter © 2011 Elsevier B.V. All rights reserved.
doi:10.1016/j.jpowsour.2011.09.066

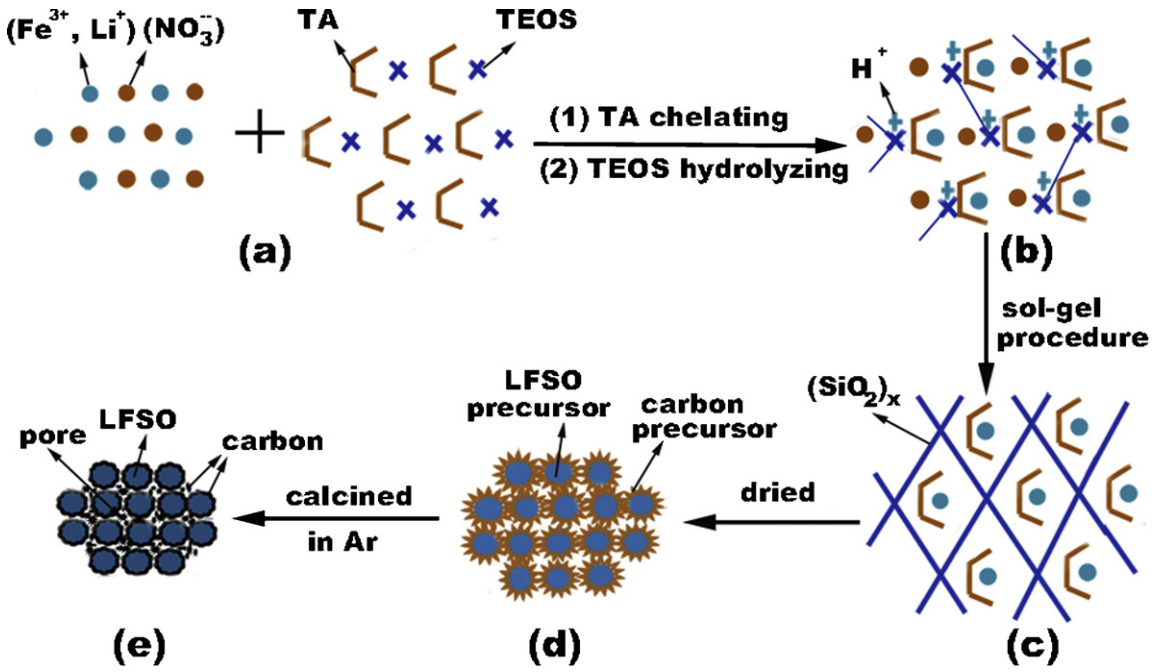

Fig. 1. Schematic illustration of the preparation of porous Li_2FeSiO_4/C nanocomposite (LFSO refers to Li_2FeSiO_4). First, TA complex with metal ions and release the dissociated H^+, which participate in catalyzing the hydrolysis of TEOS (a → b). Second, through a sol–gel procedure (b → c), the wet gel composite is further dried to remove the extra solvent (c → d). During the sintering process, the pyrolysis of the carbon precursor in Ar generates porous Li_2FeSiO_4/C (d → e).

2. Experimental

2.1. Materials synthesis

The preparation of Li_2FeSiO_4/C composite was performed through a sol–gel route and the synthetic procedures are schematically illustrated in Fig. 1. All reagents in this study were of analytical grade and used as-received unless stated. In a typical synthesis, stoichiometric amounts of TA and tetraethyl orthosilicate (TEOS) were first dispersed in ethanol. A deionized water solution with the dissolving of stoichiometric amounts of $Fe(NO_3)_3{\cdot}9H_2O$ and $LiNO_3$ was added under continuous stirring. The mixture was stirred at 60 °C for 2 h in airtight system to avoid the volatilization of the solvent. Then, the solvent was evaporated at the same temperature under magnetic stirring until a clear gel was formed. After being dried at 80 °C for 2 h, the dry gel was ground to powders. Finally, the gel powders were treated at 350 °C for 2 h and then 600 °C for 8 h in a flowing argon atmosphere, while the exhausting gas was absorbed by diluted NaOH solution. By altering the molar ratio of TA/Li_2FeSiO_4 to 2:1, 3:1 and 4:1, the as-prepared samples were labeled as S1, S2 and S3 respectively.

2.2. Materials characterization

The structures of the as-synthesized samples were characterized by powder X-ray diffraction (XRD, RigakuD/max-2500 X-ray generator, Cu Kα radiation), transmission electron microscopy (TEM, Philips Tecnai FEI, 200 kV), and Raman spectroscopy (DXR, ThermoFisher Scientific, 532 nm). To analyze the exact structure of the as-prepared Li_2FeSiO_4, Rietveld refinement program RIETAN-2000 was utilized [17]. The morphologies of the samples were observed by scanning electron microscopy (SEM, Nanosem 430, Field Emission, 10 kV). The specific surface area and pore size distribution were analyzed by Brunauer–Emmett–Teller (BET) nitrogen adsorption–desorption measurement (Japan, BELSORP-Mini). The weight ratio of the coated carbon of the sample was tested by using elemental analyzer (German, VarioEL). The conductivity of the

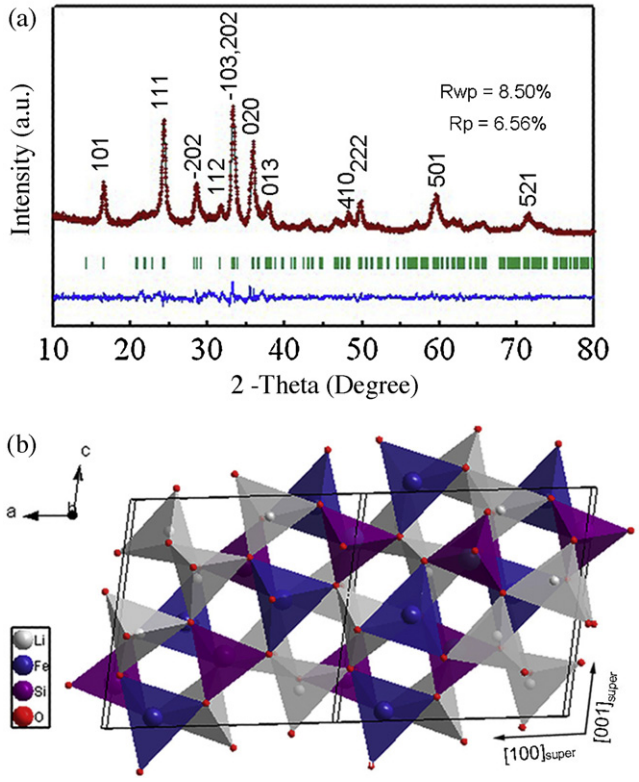

Fig. 2. (a) Rietveld refined XRD pattern (green line) of the as-prepared porous Li_2FeSiO_4/C nanocomposite with experimental data (red dots), Bragg positions (green makers) and difference curve (blue line). (b) The determined super cell structure for Li_2FeSiO_4, which is composed of alternating pairs of FeO_4 (blue) and SiO_4 (purple) tetrahedral along the direction of $[\bar{1}\,0\,1]_{super}$. (For interpretation of the references to color in this figure legend, the reader is referred to the web version of the article.).

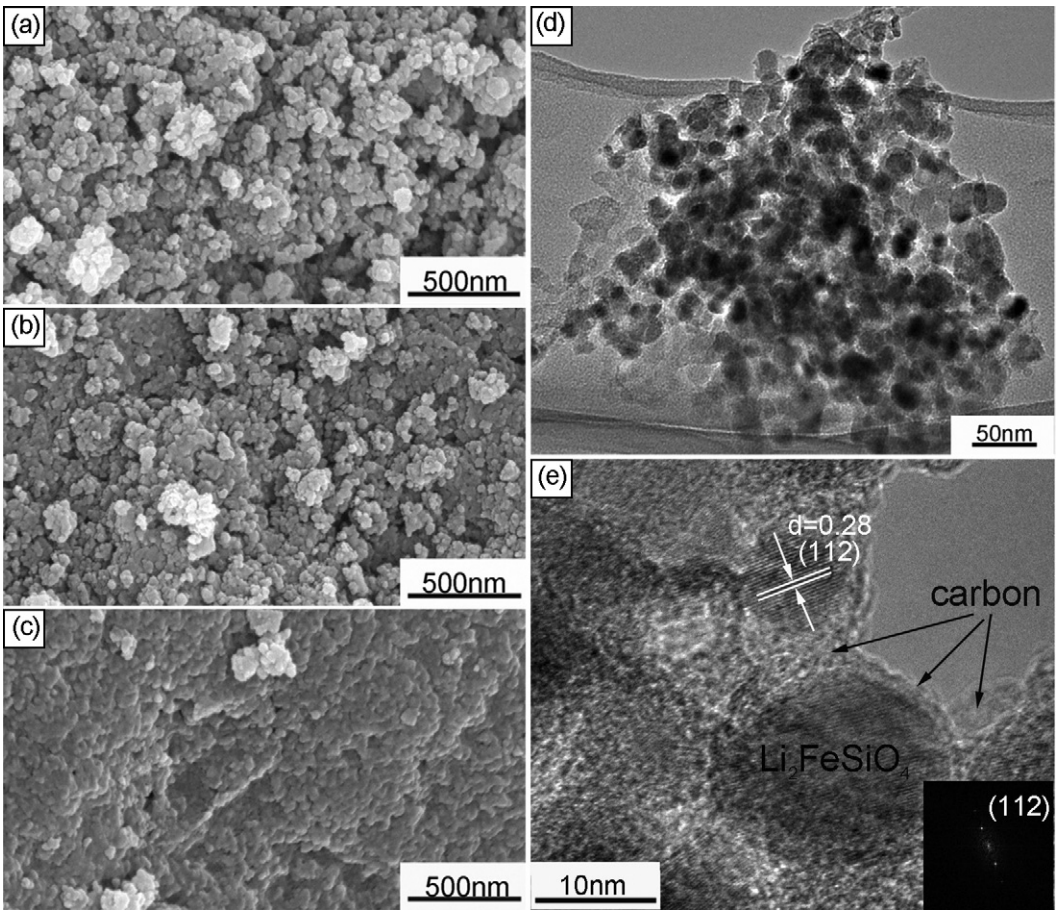

Fig. 3. SEM images of (a) S1, (b) S2 and (c) S3. TEM (d) and HRTEM (e) images of S2. The inset is the corresponding FFT pattern.

composite was measured by a four-probe meter detector (China, RTS-8) at room temperature. Three parallel measurements were carried out and the error of the measurement is about 5%. The packing density of the powders was measured by tapping the powder 100 times in a 2 mL cylinder as described [18].

2.3. Electrochemical measurements

Electrodes and coin (CR2032) cells were prepared following similar procedures described in our previous report [19]. The working electrodes were made from a mixture of 70 wt% of the active material (Li_2FeSiO_4/C, exposed to air atmosphere for 20 days), 20 wt% of the conducting agent (Vulcan XC-72, Cabot), and 10 wt% of the polyvinylidene difluoride (PVDF) binder. The assembled cells were cycled at different charge–discharge rates in a wide potential range of 1.5–4.8 V on a CT2001A cell test instrument (LAND Electronic Co.). The specific capacity was calculated on the basis of the amount of the active material, excluding the mass of the coated carbon. The cyclic voltammograms (CV) were performed at different scan rates with a Parstat 263A electrochemical workstation (AMTECT Company) [20]. Before recording the CVs at varied scan rates, the fresh cells

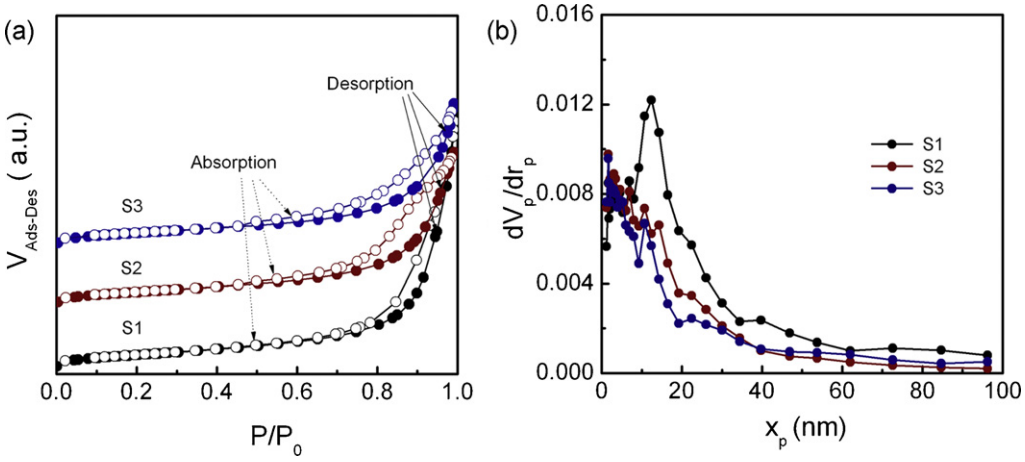

Fig. 4. (a) Nitrogen adsorption and desorption isotherms at 77 K and (b) pore-size distributions of S1, S2, and S3.

were scanned at 0.5 mV s^{-1} for 5 cycles to activate and stabilize the electrodes. All the electrochemical measurements were tested at room temperature.

3. Result and discussion

3.1. XRD analysis

According to the recent reports, Li_2FeSiO_4 performs three typical structures: a β-Li_3PO_4-based orthorhombic structure (S.G. $Pmn2_1$) [4], a monoclinic structure (S.G. $P2_1/n$) [21], and an orthorhombic structure (S.G. *Pmnb*) [22]. In this study, the selected temperatures were evaluated by thermal analysis (Fig. S1). It is found that Li_2FeSiO_4 synthesized at 600 °C shows the character of $P2_1/n$ structure (Fig. 2). No crystalline carbon can be obviously detected in the XRD pattern, revealing that the as-formed carbon layer is probably in the amorphous state or that its intensity is too low to be covered. The Rietveld refinement (Fig. 2a) shows the calculated cell parameters of $a = 8.2291$ Å, $b = 5.01436$ Å, $c = 8.2317$ Å, and $\beta = 98.6740°$, which are consistent with the previous report [21]. Fig. 2b shows the determined super cell structure of Li_2FeSiO_4. It can be seen that along the direction of $[\bar{1}\,0\,1]_{super}$, the alternating corner-shared FeO_4 and SiO_4 trigonal pyramids constitute one-dimensional chains. It is noted that large amount of organic acid contributes to high phase purity of the sample (Fig. S2).

3.2. SEM and TEM analyses

Fig. 3 displays the SEM and TEM images of S1, S2 and S3. From Fig. 3a–c, it can be seen that with the increasing of the carbon content, there is an obvious decrease of the space between the particles. Especially for S3, the particles are hardly seen due to the contact of the massive pyrolytic carbon. S2 is selected for further investigations by TEM and HRTEM (Fig. 3d and e). The typical TEM image in Fig. 3d shows the homogeneous distribution of the nanoparticles. The HRTEM image in Fig. 3e illustrates that the Li_2FeSiO_4 nanocrystals are uniformly surrounded by the carbon layer with the thickness of around 2 nm. Clear crystal lattice stripes are observed with a measured neighboring interlayer distance of 0.28 nm, which corresponds to the d-spacing of the (1 1 2) crystal plane.

3.3. BET analysis

To analyze the texture of the nanocomposites, we have measured the nitrogen adsorption–desorption isotherms of S1, S2 and S3. The determined BET specific surface areas of S1, S2 and S3 are 56.7, 64.4 and 62.1 $m^2\,g^{-1}$, respectively. There is a notable hysteretic effect between the adsorption and desorption isotherms (Fig. 4a), indicating the existence of accumulated pores [23]. The porous structures are mainly produced from the preparation process, which is due to the release of gases from the decomposition of the organic acid. The corresponding pore-size distribution curves (Fig. 4b) show that the pore sizes of the three samples mainly locate between 5 and 20 nm.

3.4. Carbon and conductivity analysis

The actual content of the coated carbon, calculated grain size using Scherrer's formula, specific surface area, electronic conductivity and the packing density of S1, S2, and S3 are summarized in Table 1. The measured electronic conductivities of S1, S2 and S3 are 1.58×10^{-5}, 4.94×10^{-4} and 1.63×10^{-3} S cm^{-1}, respectively, which are much higher than that of the uncoated Li_2FeSiO_4 ($\sim 10^{-14}$) [24]. In general, the electronic conductivity of Li_2FeSiO_4/C composite can be increased by several orders of magnitude with the increasing of the carbon content. However, the coating of carbon leads to a decrease of the packing density of the powders, which is unfavorable to its actual applications as the electrode material.

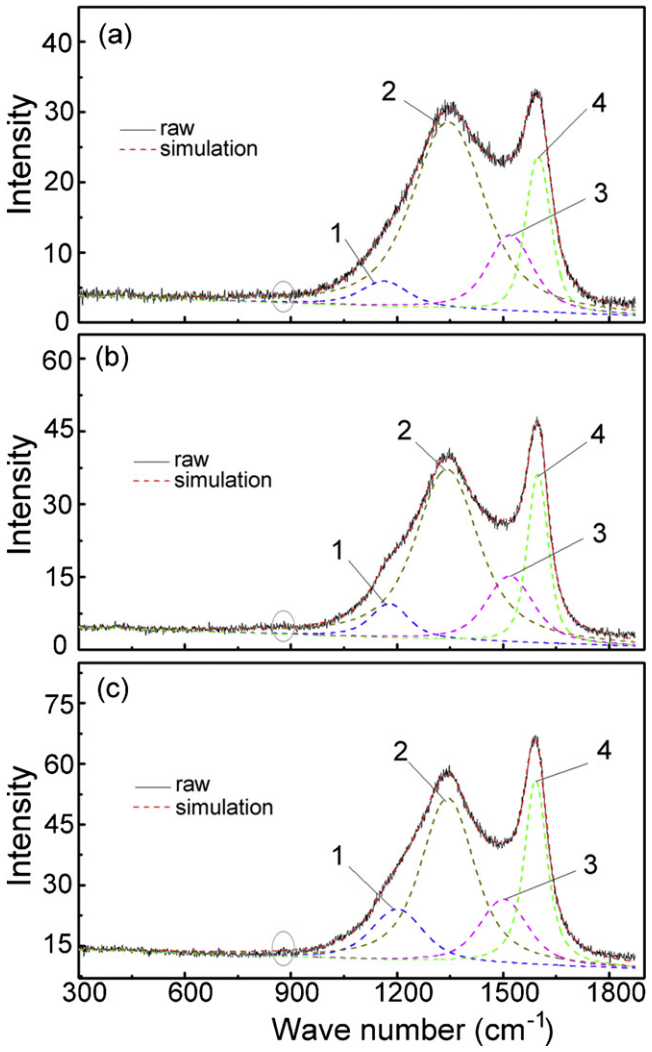

Fig. 5. Raman spectrograms of (a) S1, (b) S2, and (c) S3. The two broad bands of each sample can be deconvoluted into dotted-line four peaks (Peak 1, Peak 2, Peak 3, and Peak 4) from a Gaussian numerical simulation, which are attributed to four vibration modes of the coated carbon. The SiO_4 structure should be around 890 cm^{-1} marked with the cycle.

Fig. 5 shows the Raman spectroscopy of S1, S2, and S3. The Raman signals at around 1350 cm^{-1} (Peak 2) and 1590 cm^{-1} (Peak 4) are D (disordered) band and G (graphite) band of sp^2 type carbon, while the others at around 1180 cm^{-1} (Peak 1) and 1510 cm^{-1} (Peak 3) are related to sp^3 type carbon [25,26]. The integrated area ratio of sp^3 and sp^2 (A_{sp^3}/A_{sp^2}) can be used to roughly estimate the relatively content of the graphite carbon. The low A_{sp^3}/A_{sp^2} ratio (0.28, 0.30 and 0.42 for S1, S2 and S3 respectively) indicates that large amount of the coated carbon in all samples exists in sp^2 type. Additionally, the I_D/I_G ratio (intensity ratio of D and G bands) of S1, S2 and S3 are fitted to 1.12, 0.99 and 0.88 respectively, which can be used to evaluate the graphitization degree of the composite. The smallest I_D/I_G ratio of S3 is associated with the highest electronic conductivity [27], agreeing with the measured results in Table 1.

3.5. Capacity and rate properties

Fig. 6 displays the continuous charging and discharging performances of Li_2FeSiO_4/C materials at varied rates. As shown in

Table 1
The weight ratio of the coated carbon, average grain size, specific surface area, electronic conductivity and packing density of the as-prepared S1, S2, and S3.

Sample	Weight ratio of coated carbon (wt%)	Average grain size (nm)	Specific surface area ($m^2\,g^{-1}$)	Electronic conductivity ($S\,cm^{-1}$)	Packing density ($g\,cm^3$)
S1	3.12	42.3	56.7	1.58×10^{-5}	0.967
S2	8.06	31.8	64.4	4.94×10^{-4}	0.961
S3	10.79	28.9	62.1	1.63×10^{-3}	0.947

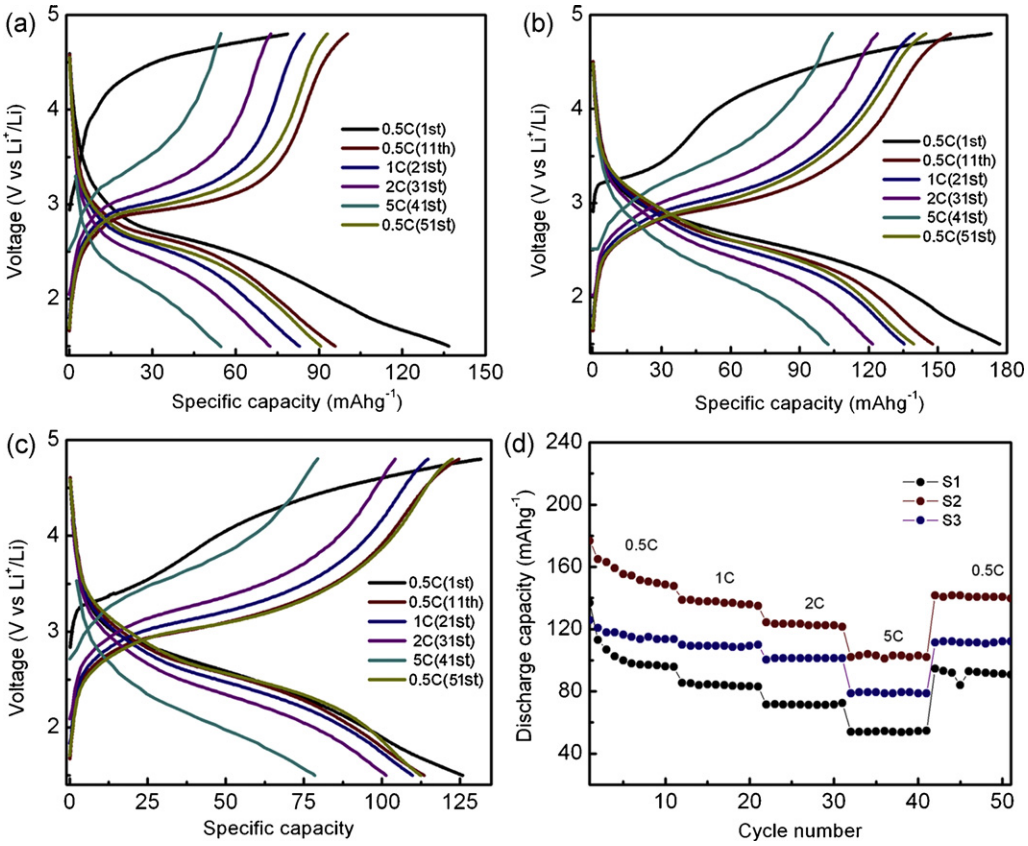

Fig. 6. Charge–discharge curves of (a) S1, (b) S2, (c) S3, and (d) their corresponding capacity performance continuously cycled at 0.5, 1, 2, 5 and 0.5 C.

Fig. 6a–c, the initial charge curve is different from the others, which has been ascribed to the structural rearrangement during the first charge process. Additionally, the initial charge capacities around 3.2 V of S1, S2, and S3 are improved with the increasing of the coated carbon. This confirms that the oxidation of Li_2FeSiO_4 with the exposition in the air is prevented [28–30]. Fig. 6d shows the full capacity changes for S1, S2, and S3 at 0.5, 1, 2 and 5 C, respectively. It can be seen that S2 shows a high capacity of 176.8 mAh g^{-1} at 0.5 C in the first cycle. This high capacity indicates that more than one electron reaction may be occurred. In spite of a large fading in the second cycle caused by some parasitic reactions, the discharge capacities perform a tendency toward stabilization in the following cycles. The high rate performance of S2 seems to be compatible with that of Li_2FeSiO_4/C nanograins [16].

Fig. 7 further shows the discharge capacities of S1, S2, and S3 at 1 C for 50 cycles. It can be seen that the carbon content dramatically affects the capacity and cyclic performance of porous Li_2FeSiO_4/C nanocomposite. In particular, S2 shows the highest initial discharge capacity of 155.3 mAh g^{-1} and a stable capacity of 132.1 mAh g^{-1} after 50 cycles. This is due to that proper content of carbon (~8.0 wt%) can enhance the conductivity of the material and thus improve the cyclic performance.

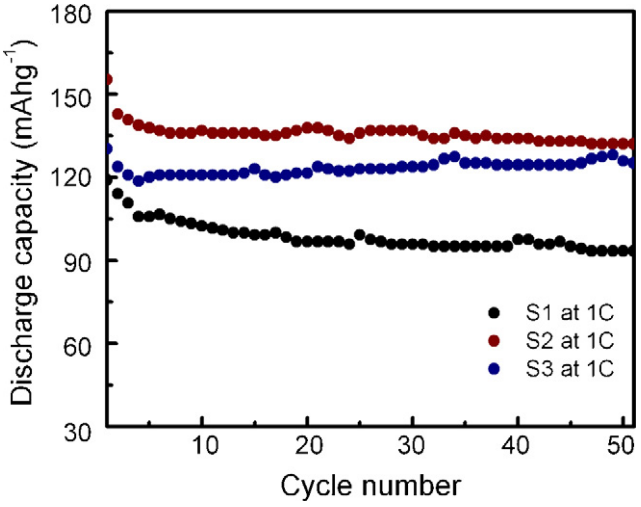

Fig. 7. The discharge capacity and cyclic performance of S1, S2 and S3, which are charged and discharged for 50 cycles between 1.5 and 4.8 V at 1 C and room temperature.

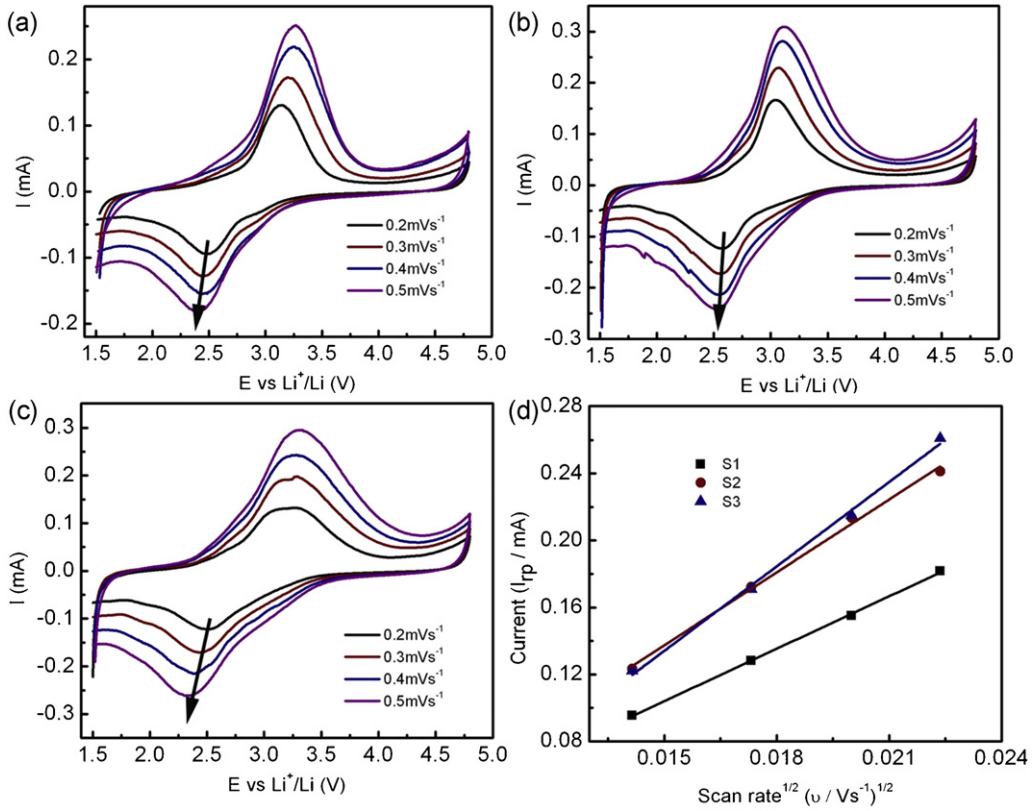

Fig. 8. Cyclic voltammograms of (a) S1, (b) S2, (c) S3 (at different scan rates), and (d) plots of the reductive peak current (I_{rp}, marked with arrows in a, b, and c) as a function of the square root of the scan rates ($\upsilon^{1/2}$) for S1, S2, and S3.

Table 2
ΔE_p at various scan rates and the Li^+ diffusion coefficiencies (D_{Li}) of the as-prepared S1, S2, and S3.

Sample	ΔE_p (V) at various scan rates (υ/V s^{-1})				Diffusion coefficient of Li^+ (D_{Li}/cm^2 s^{-1})
	0.0002	0.0003	0.0004	0.0005	
S1	0.660	0.745	0.795	0.854	7.52×10^{-13}
S2	0.464	0.518	0.568	0.602	1.46×10^{-12}
S3	0.665	0.850	0.908	0.985	1.95×10^{-12}

3.6. Cyclic voltammetry analysis

Cyclic voltammetry (CV) analysis has been carried out to understand the kinetic characteristic of porous Li_2FeSiO_4/C nanocomposite. Fig. 8a–c shows one couple of the Fe^{2+}/Fe^{3+} redox peaks. Among the three samples, S2 exhibits the smallest voltage difference (ΔE_p) at each scan rate (see details in Table 2). The diffusion coefficient of lithium ions (D_{Li}) can be calculated from a linear relationship between peak current I_p (A) and the square root of the scan rate $\upsilon^{1/2}$ ($V^{1/2}$ $s^{-1/2}$) from the CVs, according to the following equation [31]:

$$I_p = 2.69 \times 10^5 n^{3/2} A D_{Li}^{1/2} C_{Li}^* \upsilon^{1/2} \quad (1)$$

where n is the number of electrons per reaction species, A is the electrode area (1.13 cm^2 in this study), and C_{Li}^* is the bulk concentration of the lithium ion in the electrode (0.040 mol cm^{-3} for Li_2FeSiO_4). Fig. 8d shows the plot of I_p as a function of $\upsilon^{1/2}$ for S1, S2, and S3. It can be seen from Fig. 8d that there is a good linear relationship between I_p and $\upsilon^{1/2}$. The Li^+ diffusion coefficiencies are calculated and summarized in Table 2. The determined data falls within the order of 10^{-13}–10^{-12} cm^2 s^{-1}, which is comparable to the previous result (1.38×10^{-12} cm^2 s^{-1}) [32].

4. Conclusions

In summary, porous Li_2FeSiO_4/C nanocomposite, which has been prepared by a facile tartaric acid-assisted sol–gel route with a relatively short reaction time, has been applied as the cathode material of Li-ion battery. It is found that the electronic conductivity and Li^+ diffusion coefficiency have been improved by the combination of carbon coating, reduced particle size and porous structure. In particular, Li_2FeSiO_4/C nanocomposite with 8.02 wt% carbon coating shows favorable electrochemical properties such as high-rate ability and cycling stability, indicating its potential application as the cathode material of Li-ion battery.

Acknowledgements

This work was supported by the Research Programs of MOST (2011CB935904), NSFC (21076108), MOE Innovation Team (IRT0927), and Tianjin High-Tech (10ZCGHHZ01200 and 10SYSYJC27600).

Appendix A. Supplementary data

Supplementary data associated with this article can be found, in the online version, at doi:10.1016/j.jpowsour.2011.09.066.

References

[1] M. Armand, J.M. Tarascon, Nature 451 (2008) 652–657.
[2] A.K. Padhi, K.S. Nanjundaswamy, J.B. Goodenough, J. Electrochem. Soc. 144 (1997) 1188–1192.
[3] B.L. Ellis, K.T. Lee, L.F. Nazar, Chem. Mater. 22 (2010) 691–714.
[4] A. Nytén, A. Abouimrane, M. Armand, T. Gustafsson, J.O. Thomas, Electrochem. Commun. 7 (2005) 156–160.
[5] R. Dominko, J. Power Sources 184 (2008) 462–468.
[6] M.S. Islam, R. Dominko, C. Masquelier, C. Sirisopanaporn, A.R. Armstrong, P.G. Bruce, J. Mater. Chem. 21 (2011) 9811–9818.
[7] C. Sirisopanaporn, C. Masquelier, P.G. Bruce, A.R. Armstrong, R. Dominko, J. Am. Chem. Soc. 133 (2011) 1263–1266.
[8] P. Larsson, R. Ahuja, A. Nytén, J.O. Thomas, Electrochem. Commun. 8 (2006) 797–800.
[9] R. Dominko, D.E. Conte, D. Hanzel, M. Gaberšček, J. Jamnik, J. Power Sources 178 (2008) 842–847.
[10] J. Chen, F.Y. Cheng, Acc. Chem. Res. 42 (2009) 713–723.
[11] K. Karthikeyan, V. Aravindan, S.B. Lee, I.C. Jang, H.H. Lim, G.J. Park, M. Yoshio, Y.S. Lee, J. Alloys Compd. 504 (2010) 224–227.
[12] R. Dominko, M. Bele, M. Gaberšček, A. Meden, M. Remškar, J. Jamnik Electrochem. Commun. 8 (2006) 217–222.
[13] S. Zhang, C. Deng, S.Y. Yang, Electrochem. Solid-State Lett. 12 (2009) A136–A139.
[14] C. Deng, S. Zhang, B.L. Fu, S.Y. Yang, L. Ma, Mater. Chem. Phys. 120 (2010) 14–17.
[15] X.Y. Fan, Y. Li, J.J. Wang, L. Gou, P. Zhao, D.L. Li, L. Huang, S.G. Sun, J. Alloys Compd. 493 (2010) 77–80.
[16] Z.L. Gong, Y.X. Li, G.N. He, J. Li, Y. Yang, Electrochem. Solid-State Lett. 11 (2008) A60–A63.
[17] F. Izumi, T. Ikeda, Mater. Sci. Forum 198 (2000) 321–324.
[18] C.S. Li, S.Y. Zhang, F.Y. Cheng, W.Q. Ji, J. Chen, Nano. Res. 1 (2008) 242–248.
[19] H. Ma, S.Y. Zhang, W.Q. Ji, Z.L. Tao, J. Chen, J. Am. Chem. Soc. 130 (2008) 5361–5367.
[20] F. Cheng, J. Shen, B. Peng, Y. Pan, Z. Tao, J. Chen, Nat. Chem. 3 (2011) 79–84.
[21] S.I. Nishimura, S. Hayase, R. Kanno, M. Yashima, N. Nakayama, A. Yamada, J. Am. Chem. Soc. 130 (2008) 13212–13213.
[22] C. Sirisopanaporn, A. Boulineau, D. Hanzel, R. Dominko, B. Budic, A.R. Armstrong, P.G. Bruce, C. Masquelier, Inorg. Chem. 49 (2010) 7446–7451.
[23] E.P. Barrett, L.G. Joyner, P.P. Halenda, J. Am. Chem. Soc. 73 (1951) 373–380.
[24] A. Kokalj, R. Dominko, G. Mali, A. Meden, M. Gaberšček, J. Jamnik, Chem. Mater. 19 (2007) 3633–3640.
[25] X.M. Liu, Z.D. Huang, S. Oh, P.C. Ma, P.C.H. Chan, G.K. Vedam, K. Kang, J.K. Kim, J. Power Sources 195 (2010) 4290–4296.
[26] M.M. Doeff, Y.Q. Hu, F. McLarnon, R. Kostecki, Electrochem. Solid-State Lett. 6 (2003) A207–A209.
[27] A.C. Ferrari, J. Robertson, Phys. Rev. B 61 (2000) 14095–14107.
[28] R. Dominko, I. Arčon, A. Kodre, D. Hanžel, M. Gaberšček, J. Power Sources 189 (2009) 51–58.
[29] A. Nytén, M. Stjerndahl, H. Rensmo, H. Siegbahn, M. Armand, T. Gustafsson, K. Edström, J.O. Thomas, J. Mater. Chem. 16 (2006) 3483–3488.
[30] C. Deng, S. Zhang, Y. Gao, B. Wu, L. Ma, Y.H. Sun, B.L. Fu, Q. Wu, F.L. Liu, Electrochim. Acta 56 (2011) 7327–7333.
[31] Y. Jin, C.P. Yang, X.H. Rui, T. Cheng, C.H. Chen, J. Power Sources 196 (2011) 5623–5630.
[32] L.M. Li, H.J. Guo, X.H. Li, Z.M. Wang, W.J. Peng, K.X. Xiang, X. Cao, J. Power Sources 189 (2009) 45–50.